catalysts

MDPI

Article

Biochar-Supported FeS/Fe_3O_4 Composite for Catalyzed Fenton-Type Degradation of Ciprofloxacin

Yue Wang, Xiaoxiao Zhu, Dongqing Feng, Anthony K. Hodge, Liujiang Hu, Jinhong Lü and Jianfa Li *

Department of Chemistry, Shaoxing University, Shaoxing 312000, China; wangyue835@163.com (Y.W.); mymondy@163.com (X.Z.); fengdongqing@yeah.net (D.F.); hodgekanthony2016@gmail.com (A.K.H.); huliujiang@163.com (L.H.); lujhong@aliyun.com (J.L.)

* Correspondence: ljf@usx.edu.cn

Received: 29 October 2019; Accepted: 11 December 2019; Published: 13 December 2019

Abstract: The Fenton-type oxidation catalyzed by iron minerals is a cost-efficient and environment-friendly technology for the degradation of organic pollutants in water, but their catalytic activity needs to be enhanced. In this work, a novel biochar-supported composite containing both iron sulfide and iron oxide was prepared, and used for catalytic degradation of the antibiotic ciprofloxacin through Fenton-type reactions. Dispersion of FeS/Fe_3O_4 nanoparticles was observed with scanning electron microscopy-energy dispersive X-ray spectroscopy (SEM-EDS) and transmission electron microscopy (TEM). Formation of ferrous sulfide (FeS) and magnetite (Fe_3O_4) in the composite was validated by X-ray diffraction (XRD) and X-ray photoelectron spectroscopy (XPS). Ciprofloxacin (initial concentration = 20 mg/L) was completely degraded within 45 min in the system catalyzed by this biochar-supported magnetic composite at a dosage of 1.0 g/L. Hydroxyl radicals (·OH) were proved to be the major reactive species contributing to the degradation reaction. The biochar increased the production of ·OH, but decreased the consumption of H_2O_2, and helped transform Fe^{3+} into Fe^{2+}, according to the comparison studies using the unsupported FeS/Fe_3O_4 as the catalyst. All the three biochars prepared by pyrolysis at different temperatures (400, 500 and 600 °C) were capable for enhancing the reactivity of the iron compound catalyst.

Keywords: biochar; iron mineral; heterogeneous catalysts; antibiotic; advanced oxidation processes; water treatment; organic pollutants; Fenton reactions

1. Introduction

Biochar is a kind of carbonaceous material obtained by pyrolysis of biomass feedstock, such as wood processing residues and agricultural wastes. Based on the abundant feedstock sources and flexible preparation processes, the biochar with diverse functions can be developed and used in various processes for the removal of pollutants from water [1,2]. For example, the porous biochar with high specific surface area is a good adsorbent of organic pollutants [3,4], while the biochar rich in alkalis is more suitable for the precipitation of heavy metals (e.g., Pb^{2+} and Cd^{2+}) [5,6]. Due to its low cost, high surface area and good stability, biochar is a promising supporting material comparable with other carbons [7,8], and has been applied to enhance the performance of iron or iron minerals in environmental remediation. First, the biochar can disperse the zero-valent iron nanoparticles and prevent their aggregation, so that the removal efficiency of heavy metals (e.g., Cr(VI) and As(V)) was significantly improved [9,10]. Second, the biochar-supported nanoscale zero-valent iron has shown to be an efficient catalyst for the Fenton-type oxidation of organic pollutants, such as trichloroethylene [11,12], bisphenol A [13], sulfamethazine [14] and ciprofloxacin [15].

Biochar can activate the decomposition of hydrogen peroxide (H_2O_2) or persulfates to produce reactive oxygen species (ROSs) such as hydroxyl radicals (·OH) or sulfate radical anions ($SO_4{\cdot}^-$), which in turn can be used for oxidation of pollutants [16–19]. So, biochar is different from those inactive supporting materials, such as clays, that do not react with H_2O_2. Third, the magnetic biochar containing magnetite (Fe_3O_4) is the most popular biochar-based composite of iron compounds. In comparison to ordinary biochar, the magnetic biochar is easier to be separated and recycled, and showed greater ability to remove pollutants [20,21]. However, most of the previous studies about magnetic biochar focused on the adsorptive removal of pollutants [22]. Its application as the catalyst in Fenton-type systems has attracted the attention of researchers in the most recent years [23–25]. The previous research results indicate that the biochar-supported magnetite nanoparticles are promising catalysts for the degradation of refractory pollutants such as polycyclic aromatic hydrocarbons [24,25] and antibiotics [26–28].

In comparison to iron oxides, iron sulfides (FeS or FeS_2) are often more reactive when used as the catalysts for Fenton-type oxidation of organic pollutants, as both Fe(II) and S(-II)/S(-I) are electron donors for the activation of H_2O_2 [29–31]. FeS is the main component of Mackinawite, a common iron mineral that exists extensively in soil. FeS is also easily synthesized at mild conditions. Recent studies found that FeS is effective for activation of both H_2O_2 and persulfate, for the Fenton-type oxidation of 2,4-dichlorophenoxyacetic acid [32] and p-chloroaniline [33]. However, FeS particles prepared using ordinary methods tend to aggregate, which diminishes the active sites available for surface reactions [34]. Dispersion of FeS particles on biochar has been reported to increase its reactivity for more efficient immobilization of Cr(VI) [35,36]. However, till now there have hardly been any reports in literature about the performance of biochar-based FeS composites for the Fenton-type degradation of pollutants.

In this work, a novel biochar-supported composite containing nanosized FeS and Fe_3O_4 was prepared, and used for catalytic degradation of an organic pollutant through Fenton-type reactions. Ciprofloxacin, a common antibiotic that is frequently found in polluted water, was used as the pollutant model [37–39]. FeS was used here for catalyzing Fenton-type reactions, while Fe_3O_4 for giving the composite magnetism besides catalyzing the reactions. To the best of our knowledge, the combination of both iron sulfide and iron oxide with biochar has never been reported previously. The biochar-supported composite was characterized by scanning electron microscopy-energy dispersive X-ray spectroscopy (SEM-EDS), transmission electron microscopy (TEM), X-ray diffraction (XRD) and X-ray photoelectron spectroscopy (XPS). Its performance on the removal of ciprofloxacin was evaluated by batch degradation experiments, and compared with the unsupported FeS/Fe_3O_4 composite. The reactive oxygen species (ROS) in the Fenton-type systems were investigated, and the influence of biochar and reaction conditions was discussed.

2. Results and Discussion

2.1. Characterizations of the Biochar-Supported Composite

The SEM image in Figure 1a shows the smooth surface of biochar pieces, and that in Figure 1b indicates the rough surface of unsupported FeS/Fe_3O_4 particles with size ranged from 2–30 μm. The loading of iron compound on the biochar did not change the shape of biochar particles (Figure 1c), which have a size of <150 μm in overall. Dispersion of FeS/Fe_3O_4 particles on the biochar can be found in the biochar-supported composite (FeS/Fe_3O_4@BC500), according to that shown in Figure 1c,d, as most of the iron compound particles in the supported composite have a size of <10 μm. The TEM image in Figure 1e further proves the dispersion of nanosized FeS/Fe_3O_4 particles on biochar, while these nanoparticles would aggregate together without the support of biochar as that shown in Figure 1f. The SEM-EDS analysis results (Figure S1) demonstrate that the wood-derived biochar is composed only by C and O, as well as H, according to the elemental analysis results (C 85.3%, O 8.61% and H

2.39% by mass for BC500). No other elements were observed in this biochar, which makes it different from those biochars rich in inorganic minerals [40,41].

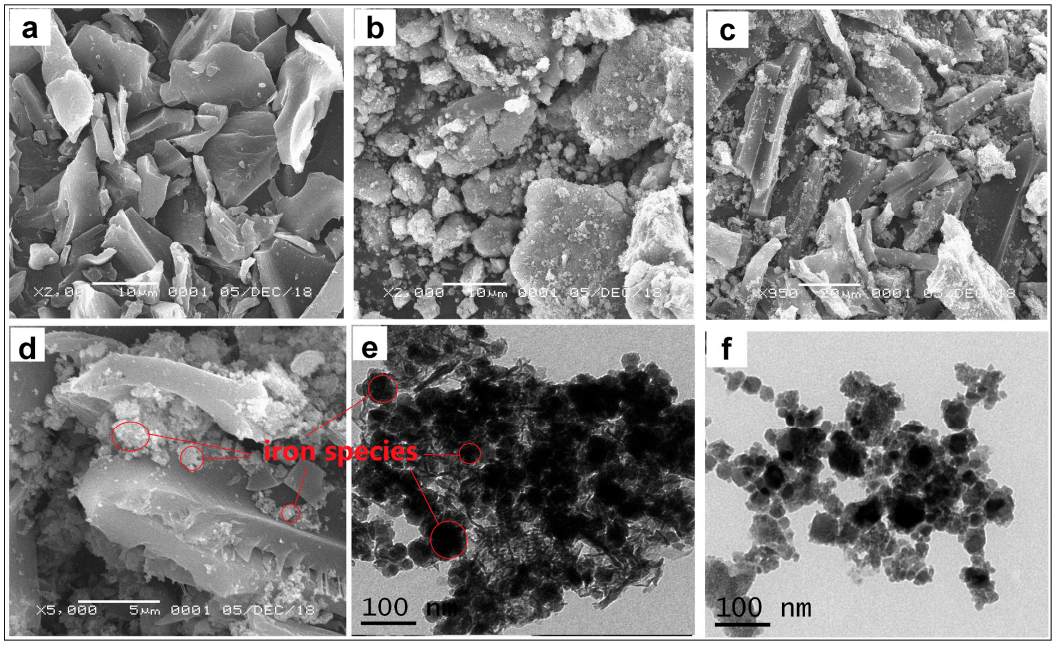

Figure 1. Scanning electron microscopy (SEM) images of (**a**) BC500 biochar (×2000), (**b**) FeS/Fe_3O_4 sample (×2000), (**c**) FeS/Fe_3O_4@BC500 composite (×950), and (**d**) FeS/Fe_3O_4@BC500 composite (×5000). TEM images of (**e**) FeS/Fe_3O_4@BC500 composite, and (**f**) FeS/Fe_3O_4 sample.

Further, no element other than Fe, O and S was observed on the unsupported FeS/Fe_3O_4 sample (Figure S1), indicating its high purity. The EDS analysis result indicates that the S content on the FeS/Fe_3O_4 surface (2.59% by mass) is much lower than that calculated (18.2% by mass) from the theoretical composition (FeS:Fe_3O_4 = 1:1 by mass). This difference should be resulted from the specific preparation procedure of FeS/Fe_3O_4 composite in this work. FeS was synthesized first and formed the inner core of the composite, while Fe_3O_4 deposited itself on the outer surface of these composite particles, accompanying with partial exposure of FeS. Therefore, the higher O content and lower S content were measured with the EDS technique that is a semi-quantitative tool to measure surface composition. The similar EDS result, namely the S content (2.52% by mass) lower than the theoretical value, was obtained on the biochar-supported composite (FeS/Fe_3O_4@BC500) (Figure S1). Here, the theoretical S content should be 6.06% by mass according to the composition of the composite (FeS:Fe_3O_4:BC500 = 1:1:4 by mass). The outer surface composing of iron oxide (Fe_3O_4) is beneficial for the stability of our catalyst in open air, as Fe_3O_4 is more resistant to oxidation by air than FeS.

The uniform distribution of S, O and Fe elements according to the EDS mapping (Figure 2) implies the formation of both iron sulfide and iron oxide that are further identified by XRD analysis (Figure 3a). The peaks belonging to both Fe_3O_4 and FeS were observed on FeS/Fe_3O_4 and FeS/Fe_3O_4@BC500 samples. The fewer and weaker peaks of FeS are related to the fact that most of the FeS is located in the inner core of particles, as discussed above about the SEM-EDS results. XPS analysis (Figure 3b) further proves the formation of two iron compounds. As that can be seen, the Fe 2p peaks at 710.1 and 711.4 eV are ascribed to the binding energies of Fe(II) of FeS and Fe_3O_4, respectively, and the S 2p peaks at 161.9 and 163.5 eV correspond to the binding energy of S^{2-} and S_n^{2-}. The peaks belonging to S^0 and S–O should be resulted from the partial oxidation of S^{2-} after exposure to air. Such oxidation may also lead to the weak signals of the S element in EDS analysis (Figure 2) and the weak FeS signal in XRD analysis (Figure 3a). The formation of Fe_3O_4 endows the magnetism, as the FeS/Fe_3O_4@BC500 powder was attracted by a magnet according that shown in Figure 3c.

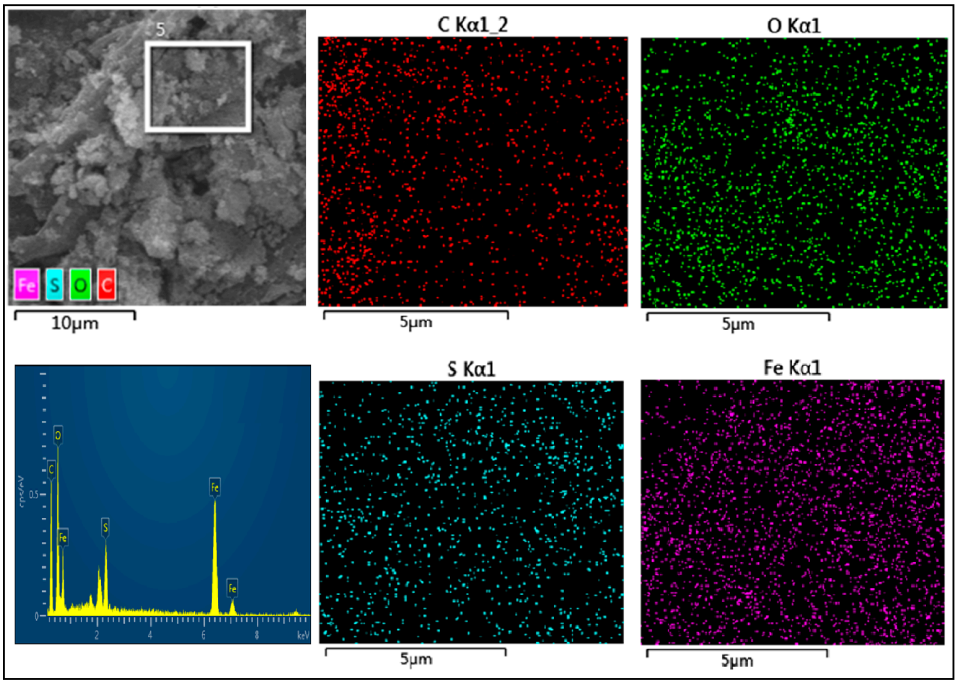

Figure 2. Electron microscopy-energy dispersive (EDS) mapping of C, O, S and Fe elements on the surface of the FeS/Fe_3O_4@BC500 composite.

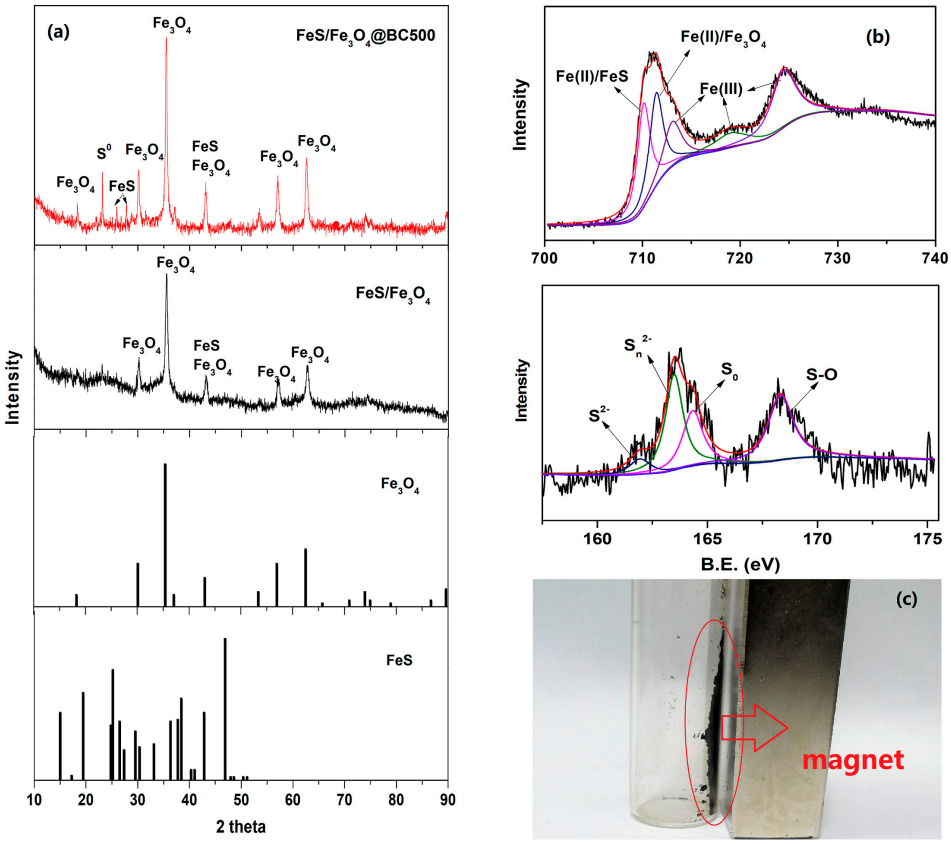

Figure 3. **(a)** X-ray diffractometry (XRD) patterns of the FeS/Fe_3O_4 and FeS/Fe_3O_4@BC500 samples; (**b**) XPS spectra of Fe 2p and S 2p regions of the FeS/Fe_3O_4@BC500 composite; and (**c**) the photo of FeS/Fe_3O_4@BC500 composite attracted by magnet.

2.2. Comparison of Various Catalysis Systems for Removal of Ciprofloxacin

The removal of ciprofloxacin by Fenton-type systems using various catalysts, including FeS/Fe_3O_4@BC500 composite, BC500 biochar and the FeS/Fe_3O_4 sample, is shown in Figure 4a. Here the dosages of iron compound (FeS/Fe_3O_4) and biochar (BC500) were set at 0.33 g/L and 0.67 g/L, respectively, equivalent to the theoretical contents in 1.0 g/L of FeS/Fe_3O_4@BC500 (1:1:4). The results of control experiments without the addition of H_2O_2 are also included in the same figure, and at least 20% of ciprofloxacin was removed by the catalysts alone in the initial stage (<2 min). The removal of ciprofloxacin by BC500 alone should be attributed to adsorption, as the biochar has a high specific surface area of 298.8 m^2/g. However, there was more ciprofloxacin removed by the two iron-containing samples (FeS/Fe_3O_4 and FeS/Fe_3O_4@BC500) than that by the biochar alone, despite that the specific surface areas of FeS/Fe_3O_4 (32.5 m^2/g) and FeS/Fe_3O_4@BC500 (120.6 m^2/g) are much smaller than the BC500 biochar. The reason should be related to the degradation of ciprofloxacin in these two systems, besides surface adsorption. Both iron sulfide and magnetite have been reported to be capable for activating dissolved O_2 in water, which results in the production of hydroxyl radicals (·OH) that are highly reactive for oxidative degradation of organic compounds [42–44]. For validating such a guess, the removal of ciprofloxacin by FeS/Fe_3O_4 or FeS/Fe_3O_4@BC500 alone was conducted under nitrogen atmosphere. Fewer pollutants were removed under nitrogen atmosphere than in the open air (Figure S2a), confirming the contribution of dissolved O_2 to the degradation of ciprofloxacin. Further, there was still a significant part (~20%) of ciprofloxacin removed by FeS/Fe_3O_4 or FeS/Fe_3O_4@BC500 in the absence of dissolved O_2 (Figure S2a), which should be attributed to adsorption. Rakshit et al. [45] has reported that ciprofloxacin was strongly adsorbed by nanomagnetite, and the quantity of ciprofloxacin adsorbed was as high as 0.04 mmol/g. The adsorption isotherms of ciprofloxacin by FeS/Fe_3O_4 and FeS/Fe_3O_4@BC500 (Figure S2b) also proved the role of these two materials as adsorbent of ciprofloxacin.

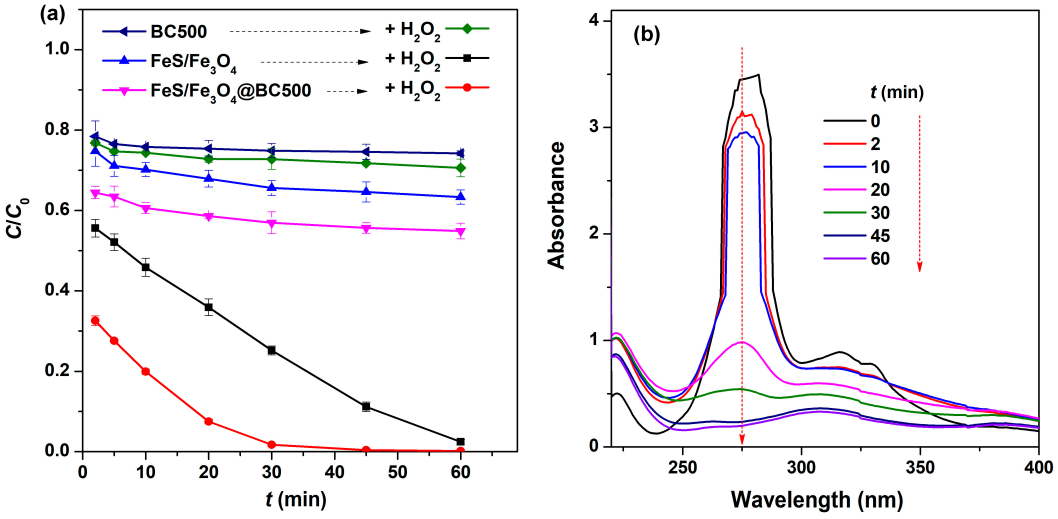

Figure 4. (**a**) Removal of ciprofloxacin (C_0 = 0.06 mmol/L) in the Fenton-type systems catalyzed by BC500 biochar, FeS/Fe_3O_4 sample and FeS/Fe_3O_4@BC500 composite, as well as the control experiments without H_2O_2; (**b**) Change of ultraviolet absorbance spectra of solution samples taken at different reaction time from the system catalyzed by FeS/Fe_3O_4@BC500 composite. Dosage of catalysts: FeS/Fe_3O_4@BC500 1.0 g/L, FeS/Fe_3O_4 0.33 g/L, or BC500 0.67 g/L; and dosage of H_2O_2 = 4.0 mmol/L. pH_0 = 3.0.

Anyway, the much quicker removal of ciprofloxacin was observed in the two H_2O_2-containing systems catalyzed by the FeS/Fe_3O_4 and FeS/Fe_3O_4@BC500 composites. In particular, nearly complete degradation of ciprofloxacin could be achieved within 45 min in the FeS/Fe_3O_4@BC500 system. The steep drop of ciprofloxacin concentration in the initial stage (<2 min) should be due to both the adsorption and degradation of ciprofloxacin. The higher removal of ciprofloxacin in the FeS/Fe_3O_4@BC500 system

than that in the FeS/Fe_3O_4 system is partially resulted from the well dispersion of FeS/Fe_3O_4 particles on biochar, because there are more reactive sites on FeS/Fe_3O_4@BC500 available for the degradation of pollutant. Further, the aqueous samples taken at various reaction times were analyzed with ultraviolet absorbance, so as to validate that the removal of ciprofloxacin was resulted from a degradation reaction. The spectra shown in Figure 4b indicate the gradual attenuation of peak absorption at ~275 nm with the reaction proceeding, accompanying with a emerging peak at 225 nm. This peak at ~275 nm is characteristic of quinoline structure in ciprofloxacin molecules. Its attenuation and disappearance after a reaction of 30 min indicates the breakdown of quinoline structure. No other strong absorbance peaks, except the emerging one at 225 nm, were observed in the solution samples after this reaction of 30 min, implying almost complete transformation of ciprofloxacin into intermediates (Figure S3) such as short-chain acids and CO_2, according to the previous research reports [37,38,46].

Repetitive experiments using the recycled composite catalysts were performed to assess their reusability (Figure 5). The dropped removal efficiency was observed in the FeS/Fe_3O_4 system since the second run, indicating the reduced catalytic activity. In comparison, the FeS/Fe_3O_4@BC500 composite maintained its catalytic activity in the second run, and the gradually decreasing removal of ciprofloxacin was found in this system after the third run. So, due to the dispersion of FeS/Fe_3O_4 on biochar, the supported FeS/Fe_3O_4@BC500 catalyst exhibited higher reusability and activity in the repetitive experiments than FeS/Fe_3O_4. The reduced activity of both catalysts should be resulted from the leaching of iron specie, because Fe content on the surface of the recycled catalysts decreased in comparison with the pristine catalysts according to SEM-EDS analysis (Figure S4 vs. Figures S1b,c). The reduced activity should also be resulted from the contamination of catalyst by reaction intermediates formed on the surface [30,32,33]. Anyway, no significant change on the mineral compositions was observed on the catalysts after reaction, according to the XRD analysis results (Figure S5).

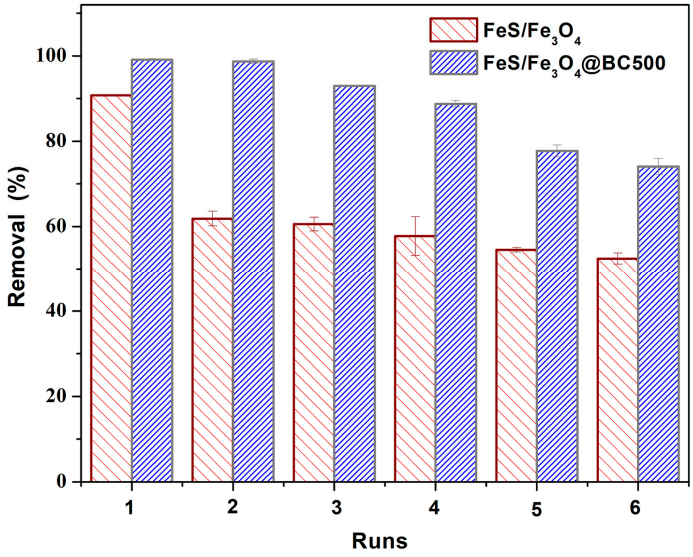

Figure 5. Removal of ciprofloxacin (C_0 = 0.06 mmol/L) in repetitive experiments after each run in the Fenton-type systems using different catalysts. Dosage: FeS/Fe_3O_4@BC500 = 1.0 g/L, FeS/Fe_3O_4 = 0.33 g/L and H_2O_2 = 4.0 mmol/L. pH_0 = 3.0.

2.3. Investigation about the Reactive Species

Methanol is a common ·OH scavenger that is frequently used for determining the major reactive oxygen species in the Fenton or Fenton-type systems. In this study, the degradation reaction of ciprofloxacin was dramatically suppressed when methanol (40 mmol/L) was added in the systems catalyzed by FeS/Fe_3O_4 and FeS/Fe_3O_4@BC500, according to the results shown in Figure 6a. The results confirm that ·OH is the reactive species that has made the major contribution for the oxidation of

ciprofloxacin, which is consistent with previous reports about the Fenton-type reactions catalyzed by iron minerals [27,29,31,32,39,47,48]. For further investigating the role of biochar, the cumulative production of ·OH in the two Fenton-type systems was measured using benzoic acid (BA) as the probe. The results in Figure 6b indicate that there were more ·OH produced in the FeS/Fe_3O_4@BC500 system than in the FeS/Fe_3O_4 system. The cumulative amount of ·OH produced after 60 min in the former system is 0.657 mmol/L, which is 45% higher than that in the later system. In contrast, much fewer consumption of H_2O_2 was observed in the FeS/Fe_3O_4@BC500 system than that in the FeS/Fe_3O_4 system (Figure 6b). Based on the molar yield of ·OH, the utilization efficiency of H_2O_2 was enhanced from 17% in the FeS/Fe_3O_4 system to 83% in the FeS/Fe_3O_4@BC500 system with the aid of biochar. The dramatically enhanced yield of ·OH should be related to the stabilization of radicals by resonance effect from aromatic carbon and/or hydroquinone/quinone structure of biochar [49], which contributed to the accumulation of persistent free radicals in biochar according to previous studies [16,17].

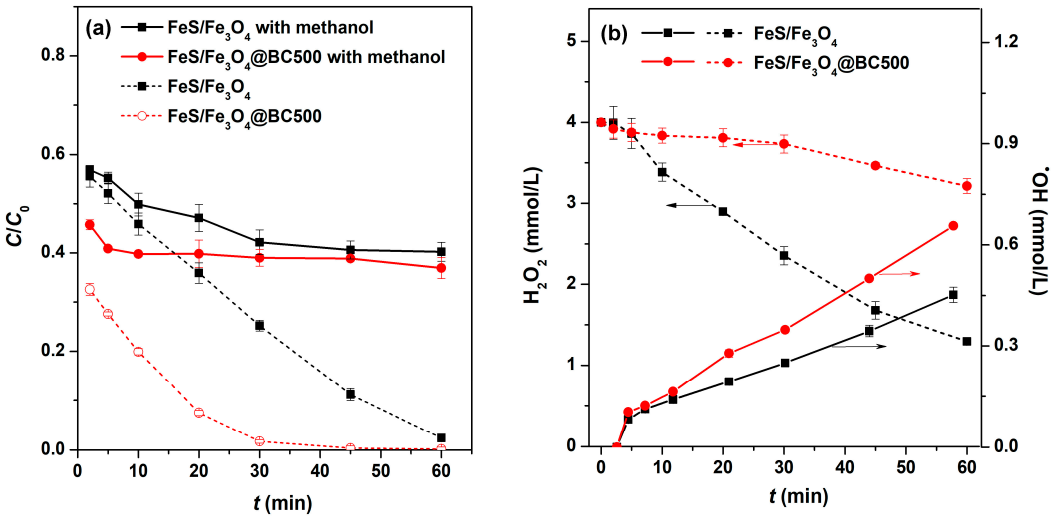

Figure 6. (**a**) Influence of methanol additive (40 mmol/L) on the removal of ciprofloxacin (C_0 = 0.06 mmol/L) in the two Fenton-type systems, and the dash lines represent those without additive; (**b**) Production of ·OH and consumption of H_2O_2 in the two systems. Dosage of catalysts: FeS/Fe_3O_4@BC500 1.0 g/L and FeS/Fe_3O_4 0.33 g/L, dosage of H_2O_2 = 4.0 mmol/L, and pH_0 = 3.0.

Furthermore, in the solution of the FeS/Fe_3O_4 system, Fe^{2+} content increased first, but then decreased in the later stage (after reaction of 30 min) (Figure 7a), which should be resulted from the oxidation of Fe^{2+}, as the total Fe in solution increased in the later stage. In contrast, both Fe^{2+} and total Fe in the solution of the FeS/Fe_3O_4@BC500 system maintained at a relatively constant level (Figure 7a). Further, the released total Fe in the FeS/Fe_3O_4@BC500 system is much fewer than that in the FeS/Fe_3O_4 system. After a reaction of 60 min, the total Fe in the FeS/Fe_3O_4@BC500 system is 2.1 mg/L, only 43% of that released in the FeS/Fe_3O_4 system (Figure 7a).

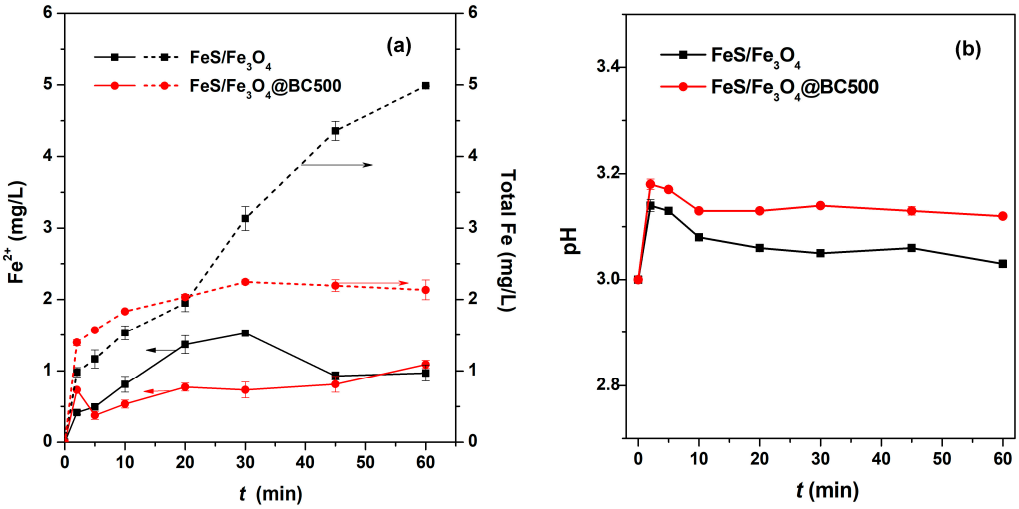

Figure 7. (**a**) Release of total Fe and Fe^{2+}, and (**b**) pH change during the reaction in the two Fenton-type systems (C_0 = 0.06 mmol/L). Dosage of catalysts: FeS/Fe_3O_4@BC500 1.0 g/L and FeS/Fe_3O_4 0.33 g/L, dosage of H_2O_2 = 4.0 mmol/L, and pH_0 = 3.0.

The results indicate the biochar-supported composite is more stable than the unsupported one, which is beneficial for reusability of the biochar-supported catalyst. The reasons should be mainly attributed to the function of biochar as an electron donor that can help transform Fe^{3+} into Fe^{2+} [50]. There are many hydroquinone (Ar–OH) and quinone groups (Ar–C=O) on the biochar according to its infrared spectra shown in Figure S6. The conversion of biochar hydroquinone and quinone groups would donate electrons that promoted the Fe^{2+}/Fe^{3+} cycle [50,51], which is beneficial for increasing the yield of ·OH at the less consumption of H_2O_2 (Figure 6b). In addition, pH change during the reaction in the two Fenton-type systems was also recorded, and results in Figure 7b indicate that pH in the FeS/Fe_3O_4@BC500 system is somewhat higher than that in the FeS/Fe_3O_4 system. The results indicate that the accelerated removal of ciprofloxacin in the former system should not attribute to the pH change, as it is well known that pH close to 3.0 is beneficial for quicker Fenton-type reactions.

2.4. The Biochar's Influence to the Removal of Ciprofloxacin

Two other biochar samples prepared at different pyrolysis temperatures (400 and 600 °C) were used instead of BC500 for preparation of the biochar-supported composites. As that can be seen in Figure 8a, all the composites have demonstrated to be more reactive than FeS/Fe_3O_4 for removal of ciprofloxacin. Among the three biochar-based composites, FeS/Fe_3O_4@BC400 shows to be less reactive than the others (Figure 8a). This should be related to ·OH production in the corresponding Fenton-type systems, because fewer ·OH radicals were produced in the system catalyzed by FeS/Fe_3O_4@BC400 (Figure 8b). The reason should be attributed to the properties of BC400 biochar different from the other two biochars. Previous studies have shown that the biochar prepared at lower temperatures (<400 °C) has more un-carbonized organic residues such as polycyclic aromatic hydrocarbons [52]. These organic residues might compete with the target pollutant (ciprofloxacin) for the consumption of reactive species [53]. The BC600 biochar alone can remove more ciprofloxacin, according to the results in Figure 8a. Such a higher removal should be resulted from the more adsorption of ciprofloxacin by this biochar that has higher specific surface area (378 m^2/g). The relatively higher reactivity of FeS/Fe_3O_4@BC500 and FeS/Fe_3O_4@BC600 composites in catalyzing the degradation of ciprofloxacin (Figure 8a) should be related to the higher aromaticity of biochar prepared at higher pyrolysis temperature. Because more aromatic structure in biochar favors the resonance stabilization of free radicals [40,54].

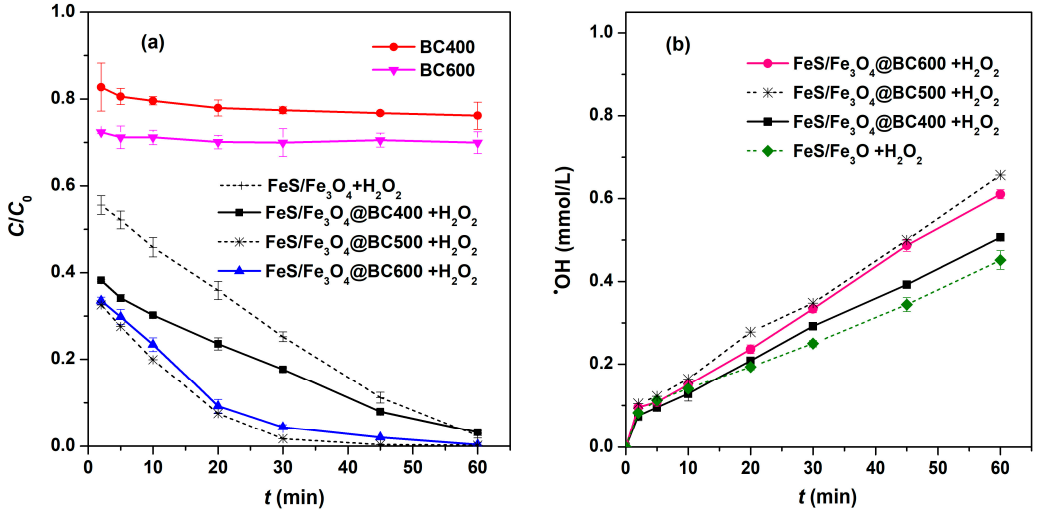

Figure 8. (**a**) Removal of ciprofloxacin (C_0 = 0.06 mmol/L) in the Fenton-type systems catalyzed by composite based on different biochar (BC400, BC500 and BC600), and the control experiments using biochar alone; (**b**) Production of ·OH in the systems using composite catalysts based on different biochar. Dosage: the composite catalyst = 1.0 g/L, the biochar = 0.67 g/L, H_2O_2 = 4.0 mmol/L. pH_0 = 3.0.

In general, the biochars prepared at temperatures other than 500 °C were also applicable as support of iron compounds for enhancing their catalytic activity, while the reasons for the different performance of biochar prepared at different temperatures deserve further investigations.

2.5. Influence of Reaction Conditions

The delayed removal of ciprofloxacin was observed with increasing pH. The much quicker removal of ciprofloxacin was obtained at pH_0 = 2.0 or 3.0 (Figure 9a), indicating that release of Fe^{2+} was the dominant factor for this Fenton-type system. As the increase of pH suppressed the dissolution of Fe^{2+} from the solid catalyst, the Fenton reactions and degradation of ciprofloxacin were slowed down. Furthermore, the optimum molar H_2O_2/ciprofloxacin ratio for removal of ciprofloxacin was in the range of 33.3 to 66.7 (and the dosage of H_2O_2 was 2 to 4 mmol/L), according to the results shown in Figure 9b. This range is 0.71 to 1.42 times the stoichiometric ratio for total mineralization of ciprofloxacin by Fenton's oxidation, which is 47 according to a previous study [46]. Fewer H_2O_2 would limit the amount of ·OH produced, while excess H_2O_2 dosage is unfavorable (Figure 9b), because the excess H_2O_2 would react with ·OH (Equation (1)). Such reaction will produce less oxidizing species (HO_2·) together with extra consumption of ·OH, so that the oxidation of ciprofloxacin by ·OH was impacted adversely.

$$H_2O_2 + \cdot OH \rightarrow HO_2\cdot + H_2O \quad (1)$$

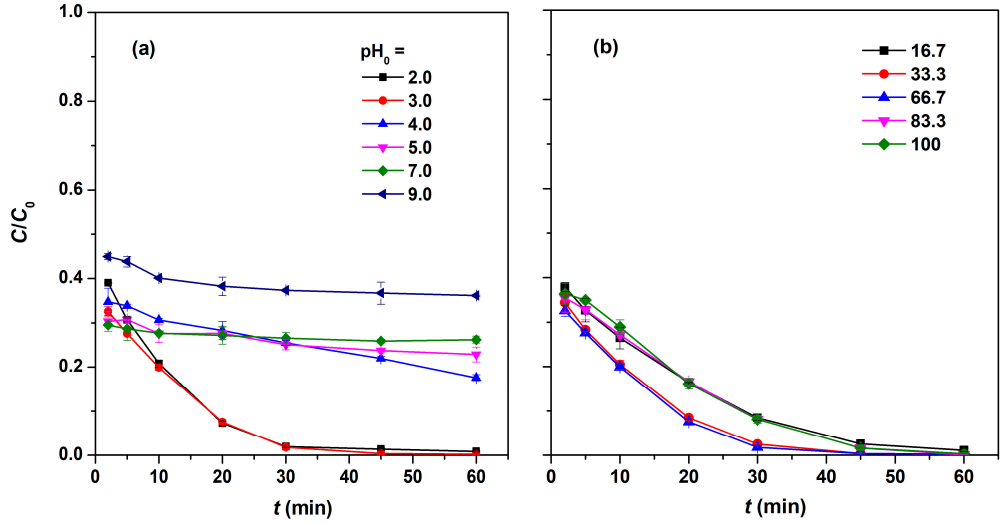

Figure 9. Removal of ciprofloxacin (C_0 = 0.06 mmol/L) in the Fenton-type system catalyzed by FeS/Fe_3O_4@BC500 (1.0 g/L) at: (**a**) different pH_0 at the same molar H_2O_2/ciprofloxacin ratio of 66.7, and (**b**) different molar H_2O_2/ciprofloxacin ratio at the same pH_0 of 3.0.

On the basis of above results and discussion about the reactive species and influencing factors, the Fenton-type reactions catalyzed by the biochar-supported FeS/Fe_3O_4 composite can be outlined. First, dissolution of Fe^{2+} from the catalyst (Equation (2)) in acidic pH was the primary step to initiate the following reaction for ·OH production (Equation (3)), so the performance of this catalyst in neutral and alkalescent pH was impacted adversely. Second, conversion of biochar hydroquinone (BCHQ) to quinone (BCQ) facilitated the regeneration of Fe^{2+} (Equation (4)), which replaced the reaction (5) essential for Fe^{2+} regeneration in the traditional Fenton system. Therefore, the extra consumption of H_2O_2 by side reactions, such as that which occurred in Equation (5), was reduced in the system catalyzed by the FeS/Fe_3O_4@BC500 composite (Figure 6b).

$$\text{BC} \equiv \text{Fe(II)} \rightarrow \text{Fe}^{2+}\text{(dissolution)} \quad (2)$$

$$\text{Fe}^{2+} + \text{H}_2\text{O}_2 \rightarrow \text{Fe}^{3+} + \text{OH}^- + \cdot\text{OH} \quad (3)$$

$$\text{Fe}^{3+} + \text{BCHQ} \rightarrow \text{Fe}^{2+} + \text{BCQ} \quad (4)$$

$$\text{Fe}^{3+} + \text{H}_2\text{O}_2 \rightarrow \text{Fe}^{2+} + \text{HO}_2\cdot + \text{H}^+ \quad (5)$$

3. Materials and Methods

3.1. Materials

Biochar was prepared by slow pyrolysis of pinewood (*Pinus radiata*) sawdust in a tube furnace (Φ 8 cm × 100 cm in length) according to the procedure reported previously [4,5,55]. The sawdust was washed with pure water, and air-dried to constant weight. The quartz vessel loaded with clean sawdust was put into the furnace filled with a continuous nitrogen flow of 200 mL/min. Then the furnace was heated to a set temperature (400, 500 or 600 °C) at a heating rate of 8 °C/min, followed by a holding time of 3.0 h. The solid residue in the furnace was taken out from the tube after the furnace was cooled to room temperature, and soaked in pure water for 24 h to remove any soluble matter from the biochar. The biochar produced at a different pyrolysis temperature is labeled as BC400, BC500 or BC600, respectively, where the suffix indicates the pyrolysis temperature in degrees Celsius. The biochar particles passing through a 100-mesh sieve (particle size <150 μm) were used in the following experiments.

Ciprofloxacin ($C_{17}H_{18}FN_3O_3$) of 98% purity was purchased from Aladdin Co. Ltd. (Shanghai, China). Ferrous sulfate heptahydrate ($FeSO_4{\cdot}7H_2O$), ferric sulfate ($Fe_2(SO_4)_3$), sodium sulfide nonahydrate ($Na_2S{\cdot}9H_2O$) and sodium hydroxide (NaOH) were all of analytical grade and purchased from Sinopharm Chemical Reagent Co., Ltd. (Shanghai, China). The 18.2 MΩ·cm pure water was obtained from the Milli-Q Gradient (Millipore, Billerica, MA, USA) pure water system and used for preparing solution of ciprofloxacin and other solutions.

3.2. Preparation of the Biochar-Supported FeS/Fe_3O_4 Composites

The biochar-supported FeS/Fe_3O_4 composite was prepared by three steps. First, the biochar (e.g., BC500) was dispersed in 150 mL of deoxygened pure water, and 0.1 mol/L Na_2S was dissolved in the dispersion, followed by dropwise addition of 34.5 mL of 0.6 mol/L $FeSO_4$ solution; thereby FeS was precipitated. Second, 38 mL of 0.15 mol/L $Fe_2(SO_4)_3$ solution was added dropwise, after then 45.5 mL of 1.0 mol/L NaOH solution was added under stirring, so that iron oxide precipitated. Third, the mixture was sealed and aged in a warm water (70 °C) bath for 48 h. The solid product was filtered out and dried in a vacuum. The as-prepared product has a mass FeS/Fe_3O_4 ratio of 1:1, which was chosen as a compromise for achieving both high catalysis reactivity and magnetism. According to our preliminary experiments, the higher FeS ratio is favorable for high reactivity, but also leads to poor magnetism. The biochar dosage used for preparing the composite follows the mass FeS/Fe_3O_4/biochar ratio of 1:1:4. Lower biochar dosage is unfavorable for the dispersion of iron species, while higher biochar dosage results in declined reactivity of the composite catalyst. The biochar-supported composites were labeled as FeS/Fe_3O_4@BC400, FeS/Fe_3O_4@BC500 and FeS/Fe_3O_4@BC600, according to the biochar used for preparing the composite. For a comparison study, the unsupported composite of mass FeS/Fe_3O_4 ratio = 1:1 was prepared by same steps without the addition of biochar.

3.3. Characterizations of the Biochar and Composites

The specific surface area (SA) of the samples (biochar and composites) was calculated using the Brunauer–Emmett–Teller (BET) method based on the N_2 adsorption/desorption isotherms that were measured at 77K in a Tristar II 3020 surface area and porosity analyzer (Micromeritics, Norcross, GA, USA), after vacuum degassing at 473 K for 6 h. Scanning electron microscopy-electron microscopy-energy dispersive (SEM-EDS) analysis was operated on a JSM-6360LV scanning electron microscope (JEOL, Tokyo, Japan), equipped with an X-act energy dispersive X-ray spectrometer (Oxford, Abingdon, UK). TEM was observed on a JEM-1011 transmission electron microscope (JEOL, Tokyo, Japan). An X-ray diffractometry (XRD) study was performed on a D/MAX 3A (Rigaku, Tokyo, Japan) equipment with CuKα radiation and a goniometer rate of 4 °/min. XPS was recorded on a Thermo ESCALAB 250 system (Waltham, MA, USA) with a monochromatized Al Kα X-ray source ($h\nu$ = 1486.6 eV) operated at a power of 150 W. The binding energies of photoelectrons were corrected by C 1s peak at 284.8 eV.

3.4. Degradation Experiments

Degradation experiments were conducted in the dark in a 100 mL conical flask containing 50 mL of ciprofloxacin solution and the catalyst. The flask was put in a thermostatic oscillator (PSE-T150A, China) at 25 ± 1 °C. H_2O_2 was quickly added into the stirring suspension to initiate the reaction. The initial concentration (C_0) of ciprofloxacin was 20 mg/L (0.06 mmol/L), and the typical dosage of H_2O_2 was 4 mmol/L, unless specified otherwise. The initial pH (pH_0) was adjusted with dilute H_2SO_4 solution to be 3.0 ± 0.1. At the predetermined reaction time (t, min), 0.3 mL of reaction solution was sampled, and put into methanol of the same volume to quench the reaction, then the solution was filtered by 0.22 μm membrane for subsequent analysis. All the experiments were carried out in triplicates.

Different catalysts, including the biochar-supported composite (e.g., FeS/Fe_3O_4@BC500) of 1.0 g/L, the FeS/Fe_3O_4 sample of 0.33 g/L (equivalent to the amount of iron species used in the supported composite), and the biochar of 0.67 g/L were used for comparison studies. The various dosages of H_2O_2 (1.0, 2.0, 4.0, 5.0 and 6.0 mmol/L, equivalent to the molar H_2O_2/ciprofloxacin ratio of 16.7, 33.3, 66.7, 83.3 and 100, respectively), and different pH_0 (2.0, 3.0, 4.0, 5.0, 7.0 and 9.0 adjusted with 0.1 mol/L H_2SO_4 or NaOH solutions) were used for investigating the influence of reaction conditions. Reusability of the catalysts was tested by separation of the solid out from the reaction system first, and the recycled catalysts were repetitively used by addition of ciprofloxacin solution and H_2O_2.

3.5. Analytical Methods

Ciprofloxacin concentration in aqueous samples was analyzed by using a HPLC system (Shimadzu LC-20A, Kyoto, Japan) equipped with a multi-wavelength UV detector. The separation was performed on an ODS-2 column (5 μm, 150 × 4.6 mm) with a flow rate of 1.0 mL /min at 25 °C. The mobile phase was a mixture of acetonitrile and 25 mmol/L H_3PO_4 solution (V/V = 16/84), and the detection wavelength was set at 275 nm (the peak absorbance of ciprofloxacin). The concentration of aqueous Fe^{2+} was measured at 510 nm using the 1,10-phenanthroline method on a UV-vis spectrophotometer (Spectrum 1920, Shanghai, China). The total aqueous Fe was examined by atomic absorption spectrometry (Shimadzu AA-7000, Japan). The accumulative production of ·OH was measured using benzoic acid as the probe, and the production of 1 mol of p-hydroxybenzoic acid (*p*-HBA) from this reaction was reported to consume 5.87 mol of ·OH [56]. The *p*-HBA was measured with HPLC using the mixture of acetonitrile/water (containing 0.15% acetic acid) = 60/40 (*v*/*v*) as the mobile phase at a flow rate of 1 mL/min, and using UV detection at 254 nm. H_2O_2 was analyzed by the Titanate method at 551 nm using the UV-vis spectrophotometer.

4. Conclusions

The biochar-supported composite containing both iron sulfide (FeS) and iron oxide (Fe_3O_4) (FeS:Fe_3O_4 = 1:1 by mass) was prepared, and has shown to be an efficient catalyst for Fenton-type oxidation of the antibiotic ciprofloxacin. The biochar made the iron species well dispersed, and enhanced its reactivity for catalyzing the degradation of ciprofloxacin. Ciprofloxacin (C_0 = 0.06 mmol/L) could be completely degraded within 45 min in the Fenton-type system catalyzed by FeS/Fe_3O_4@BC500 (1.0 g/L) with the molar H_2O_2/ciprofloxacin ratio of 33.3 to 66.7. The biochar increased the production of ·OH by 45% with a much less consumption of H_2O_2. The biochar also promoted the Fe^{2+}/Fe^{3+} cycle by acting as electron donor, which is suggested to be attributed to the hydroquinone/quinone structure in biochar. However, the reactivity of this composite catalyst depended mostly on the dissolution of Fe, which impacted its performance in neutral and alkalescent pH.

Supplementary Materials: The following are available online at http://www.mdpi.com/2073-4344/9/12/1062/s1, Figure S1: SEM-EDS results of BC500 biochar, FeS/Fe_3O_4 sample and FeS/Fe_3O_4@BC500 composite, Figure S2: Removal and adsorption isotherms of ciprofloxacin by FeS/Fe_3O_4 and FeS/Fe_3O_4@BC500 composite under nitrogen atmosphere, Figure S3: High performance liquid chromatogram of solution samples taken after different reaction time from the FeS/Fe_3O_4@BC500 system, Figure S4: SEM-EDS results of FeS/Fe_3O_4 and FeS/Fe_3O_4@BC500 composite after reaction, Figure S5: XRD patterns of FeS/Fe_3O_4 and FeS/Fe_3O_4@BC500 samples after reaction, Figure S6: Infrared spectra of BC500 biochar.

Author Contributions: Conceptualization, J.L. (Jianfa Li) and L.H.; Methodology, Y.W. and X.Z.; Investigation, Y.W., X.Z., D.F., A.K.H. and J.L. (Jinhong Lü); Validation, D.F.; Writing—Original Draft Preparation, Y.W.; Writing—Review and Editing, J.L. (Jianfa Li); Supervision, J.L. (Jianfa Li); Funding Acquisition, J.L. (Jianfa Li).

Funding: This research was funded by the National Natural Science Foundation of China, grant number 21777103.

Conflicts of Interest: The authors declare no conflict of interest.

References

1. Mukherjee, A.; Zimmerman, A.R.; Harris, W. Surface chemistry variations among a series of laboratory-produced biochars. *Geoderma* **2011**, *163*, 247–255. [CrossRef]
2. Chen, Z.; Xiao, X.; Chen, B.; Zhu, L. Quantification of chemical states, dissociation constants and contents of oxygen-containing groups on the surface of biochars produced at different temperatures. *Environ. Sci. Technol.* **2014**, *49*, 309–317. [CrossRef] [PubMed]
3. Ahmad, M.; Lee, S.S.; Rajapaksha, A.U.; Vithanage, M.; Zhang, M.; Cho, J.S.; Lee, S.-E.; Ok, Y.S. Trichloroethylene adsorption by pine needle biochars produced at various pyrolysis temperatures. *Bioresour. Technol.* **2013**, *143*, 615–622. [CrossRef] [PubMed]
4. Zhu, X.; Li, C.; Li, J.; Xie, B.; Lü, J.; Li, Y. Thermal treatment of biochar in the air/nitrogen atmosphere for developed mesoporosity and enhanced adsorption to tetracycline. *Bioresour. Technol.* **2018**, *263*, 475–482. [CrossRef] [PubMed]
5. Xu, X.; Cao, X.; Zhao, L.; Wang, H.; Yu, H.; Gao, B. Removal of Cu, Zn, and Cd from aqueous solutions by the dairy manure-derived biochar. *Environ. Sci. Pollut. Res.* **2013**, *20*, 358–368. [CrossRef] [PubMed]
6. Zhang, T.; Zhu, X.; Shi, L.; Li, J.; Li, S.; Lü, J.; Li, Y. Efficient removal of lead from solution by celery-derived biochars rich in alkaline minerals. *Bioresour. Technol.* **2017**, *235*, 185–192. [CrossRef]
7. Outsiou, A.; Frontistis, Z.; Ribeiro, R.S.; Antonopoulou, M.; Konstantinou, I.K.; Silva, A.M.; Faria, J.L.; Gomes, H.T.; Mantzavinos, D. Activation of sodium persulfate by magnetic carbon xerogels (CX/CoFe) for the oxidation of bisphenol A: Process variables effects, matrix effects and reaction pathways. *Water Res.* **2017**, *124*, 97–107. [CrossRef]
8. Soares, O.S.G.P.; Rodrigues, C.S.; Madeira, L.M.; Pereira, M.F.R. Heterogeneous Fenton-Like degradation of *p*-nitrophenol over tailored carbon-based materials. *Catalysts* **2019**, *9*, 258. [CrossRef]
9. Zhou, Y.; Gao, B.; Zimmerman, A.R.; Chen, H.; Zhang, M.; Cao, X. Biochar-supported zerovalent iron for removal of various contaminants from aqueous solutions. *Bioresour. Technol.* **2014**, *152*, 538–542. [CrossRef]
10. Diao, Z.H.; Du, J.J.; Jiang, D.; Kong, L.J.; Huo, W.Y.; Liu, C.M.; Wu, Q.H.; Xu, X.R. Insights into the simultaneous removal of Cr^{6+} and Pb^{2+} by a novel sewage sludge-derived biochar immobilized nanoscale zero valent iron: Coexistence effect and mechanism. *Sci. Total Environ.* **2018**, *642*, 505–515. [CrossRef]
11. Yan, J.; Han, L.; Gao, W.; Xue, S.; Chen, M. Biochar supported nanoscale zerovalent iron composite used as persulfate activator for removing trichloroethylene. *Bioresour. Technol.* **2015**, *175*, 269–274. [CrossRef] [PubMed]
12. Li, Z.; Sun, Y.; Yang, Y.; Han, Y.; Wang, T.; Chen, J.; Tsang, D.C. Biochar-supported nanoscale zero-valent iron as an efficient catalyst for organic degradation in groundwater. *J. Hazard. Mater.* **2020**, *383*, 121240. [CrossRef] [PubMed]
13. Liu, C.M.; Diao, Z.H.; Huo, W.Y.; Kong, L.J.; Du, J.J. Simultaneous removal of Cu^{2+} and bisphenol A by a novel biochar-supported zero valent iron from aqueous solution: Synthesis, reactivity and mechanism. *Environ. Pollut.* **2018**, *239*, 698–705. [CrossRef] [PubMed]
14. Deng, J.; Dong, H.; Zhang, C.; Jiang, Z.; Cheng, Y.; Hou, K.; Zhang, L.; Fan, C. Nanoscale zero-valent iron/biochar composite as an activator for Fenton-like removal of sulfamethazine. *Sep. Purif. Technol.* **2018**, *202*, 130–137. [CrossRef]
15. Mao, Q.; Zhou, Y.; Yang, Y.; Zhang, J.; Liang, L.; Wang, H.; Luo, S.; Luo, L.; Jeyakumar, P.; Ok, Y.S.; et al. Experimental and theoretical aspects of biochar-supported nanoscale zero-valent iron activating H_2O_2 for ciprofloxacin removal from aqueous solution. *J. Hazard. Mater.* **2019**, *380*, 120848. [CrossRef]
16. Fang, G.; Gao, J.; Liu, C.; Dionysiou, D.D.; Wang, Y.; Zhou, D. Key role of persistent free radicals in hydrogen peroxide activation by biochar: Implications to organic contaminant degradation. *Environ. Sci. Technol.* **2014**, *48*, 1902–1910. [CrossRef]
17. Fang, G.; Liu, C.; Gao, J.; Dionysiou, D.D.; Zhou, D. Manipulation of persistent free radicals in biochar to activate persulfate for contaminant degradation. *Environ. Sci. Technol.* **2015**, *49*, 5645–5653. [CrossRef]
18. Kemmou, L.; Frontistis, Z.; Vakros, J.; Manariotis, I.D.; Mantzavinos, D. Degradation of antibiotic sulfamethoxazole by biochar-activated persulfate: Factors affecting the activation and degradation processes. *Catal. Today* **2018**, *313*, 128–133. [CrossRef]
19. Magioglou, E.; Frontistis, Z.; Vakros, J.; Manariotis, I.D.; Mantzavinos, D. Activation of persulfate by biochars from valorized olive stones for the degradation of sulfamethoxazole. *Catalysts* **2019**, *9*, 419. [CrossRef]

20. Chen, B.; Chen, Z.; Lv, S. A novel magnetic biochar efficiently sorbs organic pollutants and phosphate. *Bioresour. Technol.* **2011**, *102*, 716–723. [CrossRef]
21. Wang, S.; Gao, B.; Zimmerman, A.R.; Li, Y.; Ma, L.; Harris, W.G.; Migliaccio, K.W. Removal of arsenic by magnetic biochar prepared from pinewood and natural hematite. *Bioresour. Technol.* **2015**, *175*, 391–395. [CrossRef] [PubMed]
22. Thines, K.R.; Abdullah, E.C.; Mubarak, N.M.; Ruthiraan, M. Synthesis of magnetic biochar from agricultural waste biomass to enhancing route for waste water and polymer application: A review. *Renew. Sustain. Energy Rev.* **2017**, *67*, 257–276. [CrossRef]
23. Ouyang, D.; Yan, J.; Qian, L.; Chen, Y.; Han, L.; Su, A.; Zhang, W.; Ni, H.; Chen, M. Degradation of 1, 4-dioxane by biochar supported nano magnetite particles activating persulfate. *Chemosphere* **2017**, *184*, 609–617. [CrossRef] [PubMed]
24. Dong, C.D.; Chen, C.W.; Hung, C.M. Synthesis of magnetic biochar from bamboo biomass to activate persulfate for the removal of polycyclic aromatic hydrocarbons in marine sediments. *Bioresour. Technol.* **2017**, *245*, 188–195. [CrossRef]
25. Dong, C.D.; Chen, C.W.; Kao, C.M.; Chien, C.C.; Hung, C.M. Wood-biochar-supported magnetite nanoparticles for remediation of PAH-contaminated estuary sediment. *Catalysts* **2018**, *8*, 73. [CrossRef]
26. Yi, Y.; Tu, G.; Zhao, D.; Tsang, P.E.; Fang, Z. Pyrolysis of different biomass pre-impregnated with steel pickling waste liquor to prepare magnetic biochars and their use for the degradation of metronidazole. *Bioresour. Technol.* **2019**, *289*, 121613. [CrossRef]
27. Yi, Y.; Tu, G.; Tsang, P.E.; Fang, Z. Insight into the influence of pyrolysis temperature on Fenton-like catalytic performance of magnetic biochar. *Chem. Eng. J.* **2020**, *380*, 122518. [CrossRef]
28. Nguyen, V.T.; Hung, C.M.; Nguyen, T.B.; Chang, J.H.; Wang, T.H.; Wu, C.H.; Lin, Y.L.; Chen, C.W.; Dong, C.D. Efficient heterogeneous activation of persulfate by iron-modified biochar for removal of antibiotic from aqueous solution: A case study of tetracycline removal. *Catalysts* **2019**, *9*, 49. [CrossRef]
29. Liu, W.; Wang, Y.; Ai, Z.; Zhang, L. Hydrothermal synthesis of FeS_2 as a high-efficiency Fenton reagent to degrade alachlor via superoxide-mediated Fe(II)/Fe(III) cycle. *ACS Appl. Mater. Interfaces* **2015**, *7*, 28534–28544. [CrossRef]
30. Diao, Z.H.; Liu, J.J.; Hu, Y.X.; Kong, L.J.; Jiang, D.; Xu, X.R. Comparative study of Rhodamine B degradation by the systems pyrite/H_2O_2 and pyrite/persulfate: Reactivity, stability, products and mechanism. *Sep. Purif. Technol.* **2017**, *184*, 374–383. [CrossRef]
31. Zhao, L.; Chen, Y.; Liu, Y.; Luo, C.; Wu, D. Enhanced degradation of chloramphenicol at alkaline conditions by S(-II) assisted heterogeneous Fenton-like reactions using pyrite. *Chemosphere* **2017**, *188*, 557–566. [CrossRef] [PubMed]
32. Chen, H.; Zhang, Z.; Yang, Z.; Yang, Q.; Li, B.; Bai, Z. Heterogeneous Fenton-like catalytic degradation of 2,4-dichlorophenoxyacetic acid in water with FeS. *Chem. Eng. J.* **2015**, *273*, 481–489. [CrossRef]
33. Yuan, Y.; Tao, H.; Fan, J.; Ma, L. Degradation of p-chloroaniline by persulfate activated with ferrous sulfide ore particles. *Chem. Eng. J.* **2015**, *268*, 38–46. [CrossRef]
34. Gong, Y.; Tang, J.; Zhao, D. Application of iron sulfide particles for groundwater and soil remediation: A review. *Water Res.* **2016**, *89*, 309–320. [CrossRef] [PubMed]
35. Lyu, H.; Tang, J.; Huang, Y.; Gai, L.; Zeng, E.Y.; Liber, K.; Gong, Y. Removal of hexavalent chromium from aqueous solutions by a novel biochar supported nanoscale iron sulfide composite. *Chem. Eng. J.* **2017**, *322*, 516–524. [CrossRef]
36. Lyu, H.; Zhao, H.; Tang, J.; Gong, Y.; Huang, Y.; Wu, Q.; Gao, B. Immobilization of hexavalent chromium in contaminated soils using biochar supported nanoscale iron sulfide composite. *Chemosphere* **2018**, *194*, 360–369. [CrossRef]
37. Yahya, M.S.; Oturan, N.; El Kacemi, K.; El Karbane, M.; Aravindakumar, C.T.; Oturan, M.A. Oxidative degradation study on antimicrobial agent ciprofloxacin by electro-Fenton process: Kinetics and oxidation products. *Chemosphere* **2014**, *117*, 447–454. [CrossRef]
38. Diao, Z.H.; Xu, X.R.; Jiang, D.; Li, G.; Liu, J.J.; Kong, L.J.; Zuo, L.Z. Enhanced catalytic degradation of ciprofloxacin with FeS_2/SiO_2 microspheres as heterogeneous Fenton catalyst: Kinetics, reaction pathways and mechanism. *J. Hazard. Mater.* **2017**, *327*, 108–115. [CrossRef]

39. Hassani, A.; Karaca, M.; Karaca, S.; Khataee, A.; Açışlı, Ö.; Yılmaz, B. Preparation of magnetite nanoparticles by high-energy planetary ball mill and its application for ciprofloxacin degradation through heterogeneous Fenton process. *J. Environ. Manag.* **2018**, *211*, 53–62. [CrossRef]
40. Huang, D.; Luo, H.; Zhang, C.; Zeng, G.; Lai, C.; Cheng, M.; Wang, R.; Deng, R.; Xue, W.; Gong, X.; et al. Nonnegligible role of biomass types and its compositions on the formation of persistent free radicals in biochar: Insight into the influences on Fenton-like process. *Chem. Eng. J.* **2019**, *361*, 353–363. [CrossRef]
41. Li, J.; Pan, L.; Yu, G.; Xie, S.; Li, C.; Lai, D.; Li, Z.; You, F.; Wang, Y. The synthesis of heterogeneous Fenton-like catalyst using sewage sludge biochar and its application for ciprofloxacin degradation. *Sci. Total Environ.* **2019**, *654*, 1284–1292. [CrossRef] [PubMed]
42. Cheng, D.; Yuan, S.; Liao, P.; Zhang, P. Oxidizing impact induced by mackinawite (FeS) nanoparticles at oxic conditions due to production of hydroxyl radicals. *Environ. Sci. Technol.* **2016**, *50*, 11646–11653. [CrossRef] [PubMed]
43. Zhang, P.; Yuan, S.; Liao, P. Mechanisms of hydroxyl radical production from abiotic oxidation of pyrite under acidic conditions. *Geochim. Cosmochim. Acta* **2016**, *172*, 444–457. [CrossRef]
44. Ardo, S.G.; Nélieu, S.; Ona-Nguema, G.; Delarue, G.; Brest, J.; Pironin, E.; Morin, G. Oxidative degradation of nalidixic acid by nano-magnetite via Fe^{2+}/O_2-mediated reactions. *Environ. Sci. Technol.* **2015**, *49*, 4506–4514. [CrossRef]
45. Rakshit, S.; Sarkar, D.; Elzinga, E.J.; Punamiya, P.; Datta, R. Mechanisms of ciprofloxacin removal by nano-sized magnetite. *J. Hazard. Mater.* **2013**, *246–247*, 221–226. [CrossRef]
46. Gupta, A.; Garg, A. Degradation of ciprofloxacin using Fenton's oxidation: Effect of operating parameters, identification of oxidized by-products and toxicity assessment. *Chemosphere* **2018**, *193*, 1181–1188. [CrossRef]
47. Liu, X.; Zhang, Q.; Yu, B.; Wu, R.; Mai, J.; Wang, R.; Chen, L.; Yang, S.T. Preparation of Fe_3O_4/TiO_2/C nanocomposites and their application in Fenton-like catalysis for dye decoloration. *Catalysts* **2016**, *6*, 146. [CrossRef]
48. Zhang, Y.; Tran, H.P.; Hussain, I.; Zhong, Y.; Huang, S. Degradation of p-chloroaniline by pyrite in aqueous solutions. *Chem. Eng. J.* **2015**, *279*, 396–401. [CrossRef]
49. Zhu, X.; Li, J.; Xie, B.; Feng, D.; Li, Y. Accelerating effects of biochar for pyrite-catalyzed Fenton-like oxidation of herbicide 2,4-D. *Chem. Eng. J.* **2020**, 123605. [CrossRef]
50. Qin, Y.; Zhang, L.; An, T. Hydrothermal carbon-mediated Fenton-like reaction mechanism in the degradation of alachlor: Direct electron transfer from hydrothermal carbon to Fe (III). *ACS Appl. Mater. Interfaces* **2017**, *9*, 17115–17124. [CrossRef]
51. Chen, R.; Pignatello, J.J. Role of quinone intermediates as electron shuttles in Fenton and photoassisted Fenton oxidations of aromatic compounds. *Environ. Sci. Technol.* **1997**, *31*, 2399–2406. [CrossRef]
52. Fabbri, D.; Rombolà, A.G.; Torri, C.; Spokas, K.A. Determination of polycyclic aromatic hydrocarbons in biochar and biochar amended soil. *J. Anal. Appl. Pyrolysis* **2013**, *103*, 60–67. [CrossRef]
53. Zhao, X.; Qin, L.; Gatheru Waigi, M.; Cheng, P.; Yang, B.; Wang, J.; Ling, W. Removal of bound PAH residues in contaminated soils by Fenton oxidation. *Catalysts* **2019**, *9*, 619. [CrossRef]
54. Yang, J.; Pan, B.; Li, H.; Liao, S.; Zhang, D.; Wu, M.; Xing, B. Degradation of *p*-nitrophenol on biochars: Role of persistent free radicals. *Environ. Sci. Technol.* **2015**, *50*, 694–700. [CrossRef]
55. Li, J.; Li, Y.; Wu, Y.; Zheng, M. A comparison of biochars from lignin, cellulose and wood as the sorbent to an aromatic pollutant. *J. Hazard. Mater.* **2014**, *280*, 450–457. [CrossRef]
56. Tong, M.; Yuan, S.; Ma, S.; Jin, M.; Liu, D.; Cheng, D.; Liu, X.; Gan, Y.; Wang, Y. Production of abundant hydroxyl radicals from oxygenation of subsurface sediments. *Environ. Sci. Technol.* **2016**, *50*, 214–221. [CrossRef]